CHAPTER 2

EXPERIMENTAL TECHNIQUES

The present chapter describes different synthesis procedures followed for the investigated compositions and various characterization techniques used to evaluate different properties. This chapter includes basic principles of various instruments used for data collection, and the methodology implemented to analyze these data are also briefly covered.

2.1 Sample Preparation

The controlled synthesis process is a promising way to prepare a better quality and excellent performance ferrite magnet. It plays a crucial role in the particle size band, desired chemical stoichiometry, and site position of transition elements in the compound. Several processes are available to synthesize the bulk grain form of hexaferrite materials like traditional solid-state reaction route, hydrothermal process, co-precipitation process, sol-gel process, sol-gel auto-combustion process, and pechini process. The most extensively used synthesizing process for M-type hexaferrite is traditional solid-state reaction route and sol-gel auto-combustion process, which was adopted in the present thesis to synthesize the bulk form of samples.

2.1.1 Solid-state Reaction Route (Traditional Ceramic Method)

The solid-state reaction route is the most adaptable, thermodynamically stable, as well as eco-friendly technique for preparing polycrystalline material in bulk form. Raw materials provide a wide range of selectivity from oxides, carbonates, hydroxides, sulfates, and nitrides. In this method, the stoichiometric amounts of starting materials are wet-milled by the high-energy ball milling process. The powder product depends on various parameters like the reactivity of reactants towards each other, pressure, temperature,

reaction rate, and time. A high calcination temperature is required for the desired phase formation due to a lack of diffusion among constituents elements at room temperature, followed by grinding if necessary. The high calcination temperature helps to overcome the kinetic barriers among constituents.

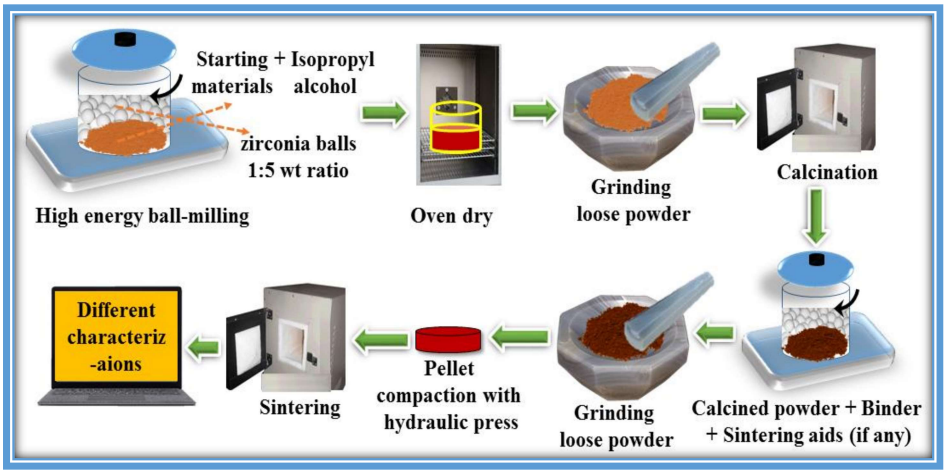

Figure 2.1 *Schematic diagram of traditional solid-state reaction route.*

Fig. 2.1 shows the flow chart of the solid-state reaction route. The stoichiometric amounts of starting materials were wet-grind with the zirconia balls by a high-energy ball-milling process. The ball milling process effectively increased the surface area of the constituents and maximized the contact between the reactants. Milling time affects the degree of homogeneity and better contact between the reactant surfaces. The outcome was then oven-dried, ground, and calcined at a high temperature. A high calcination temperature of around 1000-1350^{o}C was required to yield a metallic oxide. Further, the metallic oxide was wet-milled with the addition of a binder and other elements or sintering aids. The outcome was again oven-dried, ground for a homogeneous mixture, and pelletized in a cylindrical shape with the hydraulic press. The compacted product then undergoes the sintering process in the temperature range between 1100-1300^{o}C for few hrs to fuse the micron particles together. The process parameters like milling media, milling revolution

speed, process timing, and heat treatment were varied depending on the required properties and nature of the sample.

The solid-state reaction process was selected to prepare the **Bi_2O_3 doped $SrFe_8Al_4O_{19}$ series**. The raw materials ($SrCO_3$, Fe_2O_3, and Al_2O_3) were wet-mixed by the planetary ball mill (Model No: MBM-07, Insmart Systems, Hyderabad, India) at 600 rpm for 4 hrs using zirconia grinding media of 3 mm diameter. After the successful wet-mixing for 4 hrs, the powder was extracted by drying in an oven at 80°C. The powder was calcined at a temperature of 1150°C for 2 hrs to get the hexagonal-phase of $SrFe_8Al_4O_{19}$. Again, through the high-energy planetary ball milling process, Bi_2O_3 (sintering aid) was homogeneously mixed in 0, 1, 2, 3, 4, and 5 wt% amounts with the calcined powder at 600 rpm for 4 hrs. The resultant powders of $SrFe_8Al_4O_{19}$-xBi_2O_3 ($0 \leq x \leq 5$ wt%) were dried in an oven at 80°C. Further, 3 wt% polyvinyl alcohol was added and, consequently, granulated & pressed into cylindrical shapes (10 mm×2 mm). A pressure of about ~250 MPa was applied for palletization to encourage intimate contact between particles. Finally, pellets were sintered at different temperatures of 850°C, 950°C, 1050°C, and 1150°C for 4 hrs with a heating rate of 3°C/min in the controlled muffle furnace (OKAY Furnace, Bysakh and Co., India).

2.1.2 Sol-gel Auto-combustion Process

Sol-gel auto-combustion is a chemical process in which molecular-scale mixing of constituent elements can be attained at relatively low heating temperatures. It provides excellent homogeneity, ultrafine particles, better microstructural control, and narrow band distribution of particles. Generally, nitrates and fuels are used as precursors. As a fuel, ethylene glycol, hydrazine, oxalic acid, urea, citric acid, glycine, and acetylacetone can be used. Citric acid is the most suitable fuel due to the absence of nitrogen atoms; hence, the emission of flammable gases is less.

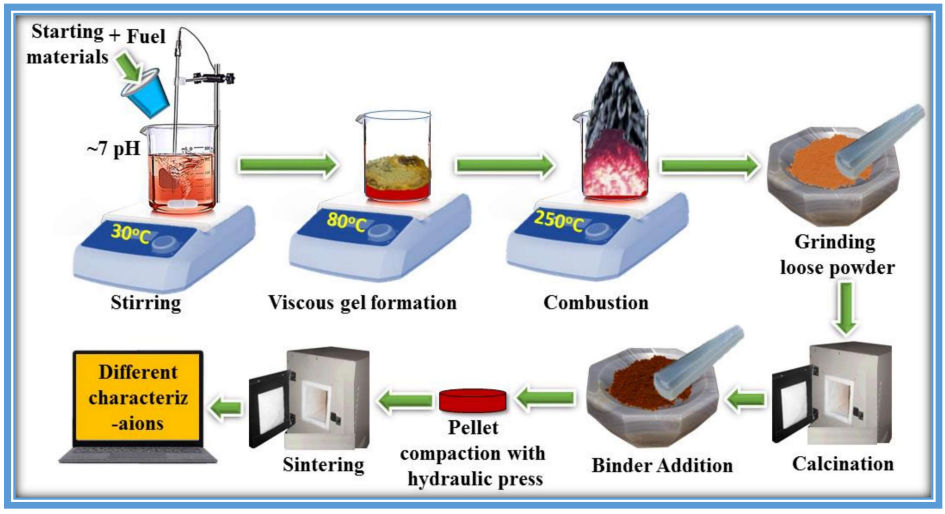

Figure 2.2 *Schematic diagram of a sol-gel auto-combustion process.*

Fig. 2.2 shows the flow chart of the sol-gel auto-combustion process. In this process, monomers were converted into a colloidal solution (sol) acting as a precursor for an integrated network (gel) of either polymer network or distinct particles. Nitrates (oxidizers) undergo a highly exothermic redox reaction with citrate ions (reducing agent) to get the desired phase. It involved the homogeneous mixing of nitrates and fuel in a 1:1 molar ratio by a magnetic stirrer at room temperature. Mixing was done by magnetic stirrer at room temperature. Ammonia solution was added dropwise to get the ~7 pH of the solution. Then, the final solution was kept at a continuous temperature of around 80-120°C until the formation of a high viscose gel. After the gel formation, the temperature was raised to ~250°C. At this stage, the combustion of NH_4NO_3 (formed during the neutralization process of solution) caused to be responsible for the driving force of the extreme exothermic reaction. It created a reaction temperature of ~227°C and ignited in an intense exothermic reaction that self-propagated entirely within 20 sec. The high speed of reaction ensured better homogeneity, and polymerization of citric acid caused the evolution of CO_2 gas resulting in the fluffy high volumetric powder. This high volumetric powder was ground and subsequently calcined around 800-1200°C, depending on the required

properties and nature of the sample. Further, the subsequent grinding, pelletization, and sintering of samples yielded the final product.

The sol-gel auto-combustion process was selected to prepare **Co-Cr substituted $SrFe_{12-x-y}Co_xCr_yO_{19}$ series, Cr-Zn substituted $Sr_{1-x}Cr_xFe_{12-x}Zn_xO_{19}$ series, Ni-Al substituted $SrFe_{12-x-y}Ni_xAl_yO_{19}$ series,** and **Al-Zn substituted $SrFe_{8-x}Al_4Zn_xO_{19}$ series**. Analytical grade $Sr(NO_3)_2$, $Fe(NO_3)_3.9H_2O$, $Co(NO_3)_2.6H_2O$, $Cr(NO_3)_3.9H_2O$, $Zn(NO_3)_2.6H_2O$, $Ni(NO_3)_2.6H_2O$, and $Al(NO_3)_3.9H_2O$ were used as the raw material according to the stoichiometry of compositions. The stoichiometric amounts of starting materials (nitrates) were weighed accordingly, and all were liquefied in a minimum amount of deionized water. The molar ratio of nitrates to citric acid was kept at 1:1. Ammonia solution was added to adjust the pH to 7. The solution was kept at 90^oC to transform into a viscose gel. After that, the temperature was raised to 250^oC to be ignited at any point. Here, combustion occurs in a self-propagating manner and results in a fluffy powder after the complete burnout. The obtained powders of all series were calcined at 1100^oC for 2 hrs with a 3^oC/min heating rate. It was mixed with 3 wt% polyvinyl alcohol and compacted in cylindrical shape (10 mm×2 mm) pellets by applying a pressure of ~250 MPa. Finally, pellets were sintered at 1250^oC for 2 hrs.

2.1.3 Heat Treatment Process

Heat treatment is an important step in synthesis process. The prominent temperature, along with suitable heating and cooling rate, is required for the appropriate reaction through which structural and morphological properties of the sample get affected. The initial heat treatment stage (calcination) is needed to form a desirable phase. At this stage, the reactive kinetic barriers of reactants are overcome by the elevated temperature yielding to the final powder of samples. The post-stage heat treatment (sintering) is needed to get the dense samples of the final product. The schematic diagram of a muffle furnace is

shown in Fig. 2.3. All samples were heat treated in a controlled muffle furnace operable till the maximum temperature of 1700°C (OKAY Furnace, Bysakh and Co., India) in air atmosphere. The temperature sensor of Pt-Rh (type – B) based thermocouple and Kanthal Super heating elements were used in the furnace. The temperature was controllable to ±1°C with the digital PID temperature controller.

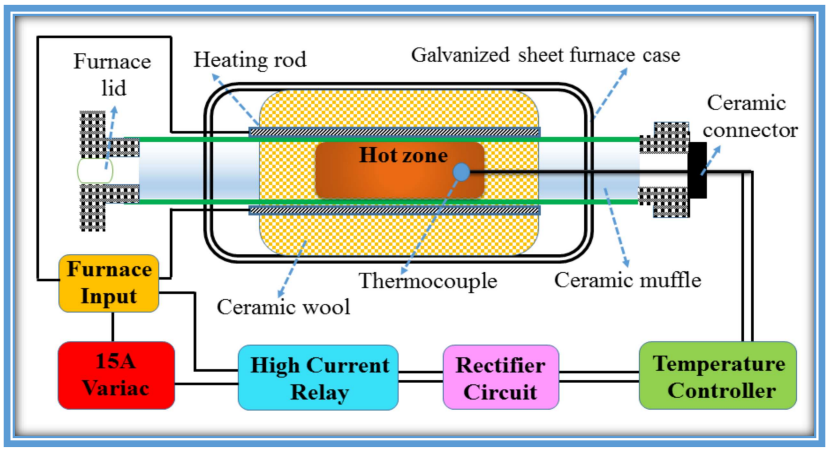

Figure 2.3 *Schematic representation of controlled muffle furnace.*

2.2 Characterization Techniques

Several standard characterization equipments is used to analyze the structural, morphological, magnetic, and dielectric properties of the samples.

2.2.1 Differential Thermal Analyzer & Thermo-gravimetric (DTA-TG)

Thermal analysis is used to study the solid-state reaction, thermal degradation reaction, and phase transition in sample. The thermo-gravimetric analyzer (TGA) collects the weight of the sample as a function of continuously increasing temperature. It consists of a sample cup coupled with a microgram balance and countered through a tare pan. Sample cup is inserted into a furnace to record the weight change with the steady-rate heating temperature, which is monitored via microgram balance and thermocouple. It gives information like phase change and thermal stability of the sample. The weight loss of

sample occurs due to the evaporation, decomposition, desorption, and reduction during the heating process; also, it may gain weight because of absorption, adsorption, and oxidation.

Differential thermal analyzer (DTA) records the temperature difference between the sample and the reference (Al_2O_3) as a function of increasing temperature. Adsorption, crystallization, oxidation, and chemisorption is the main phenomena behind the exothermic heat change while desorption, melting, vaporization, sublimation, and reduction are responsible for the endothermic heat change in the sample. Some phenomena like changes in crystal structure, breakdown reaction, and solid-state reaction could be responsible for both endothermic as well as exothermic heat change. DTA technique qualitatively analyzes the heat change and is mainly used for transition temperature detection of the sample.

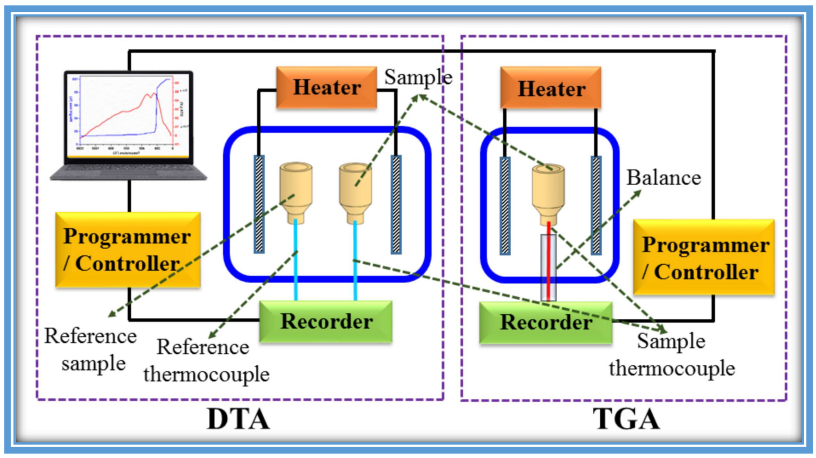

Figure 2.4 *Schematic representation of DTA and TGA.*

Fig. 2.4 shows the schematic representation of TG/DTA. The thermal decomposition of raw powder of all series was analyzed by the TG/DTA, model TA-50 WS, Shimadzu, Kyoto, Japan, at the heating rate of 10°C/min up to 1200°C temperature.

2.2.2 X-ray Diffraction (XRD)

X-ray diffraction (XRD) technique is the most vital and non-destructive technique for phase and structural identification of the material. It gives various informative data like atomic arrangement, atomic spacing, lattice parameters, average crystallite size, lattice

strain, and x-ray density of a material. The x-ray diffraction pattern is based on Bragg-Brentano geometry and is the outcome of Bragg's law. A schematic representation of Bragg-Brentano geometry (Ray diagram of XRD) and Bragg's law are shown in Fig. 2.5. In this geometry, x-ray lamp (F1) and receiving slit (F2) are equidistant from sample frame so that the diffracted x-ray beam by angle 2θ will always focus at F2 point. When a collimated monochromatic x-ray beam is incident on the sample that contains many lattice planes with an interplanar spacing of *d*, which is in order of angstrom (Å), x-ray beams get scattered by different lattice planes. According to the interplanar spacing (*d*) and incident angle (θ), some diffracted beams undergo constructive interference and give the diffraction pattern of material by satisfying Bragg's law, i.e,

$$n\lambda = 2dsin\theta \tag{2.1}$$

where n is the order of diffraction, λ is the wavelength of x-ray beam.

In the present work, structural identity was confirmed by the Rigaku Miniflex 600 benchtop x-ray diffractometer with Cu-K_α (1.5406 Å) radiation in the 2θ range of 20-80°. The diffracted x-ray beam intensity as a function of diffraction angle (2θ), i.e., diffraction pattern was recorded with an angular step size of 0.01°. Phase identification was done by matching the diffraction profile with the reference ICDD card. The ratio of lattice parameter *c/a* was used to quantify the structure type, which should be less than 3.98 for the formation of a magnetoplumbite hexagonal structure. The structural parameters such as lattice parameters (*a/b, c*), cell volume (*V*), crystallite size (*D*), lattice strain (Є), and x-ray density (χD) were calculated by Eq. (2.2), Eq. (2.3), Eq. (2.4), Eq. (2.5), and Eq. (2.6), respectively:

$$\sin^2\theta = \frac{\lambda^2}{4}\left[\frac{4\left(h^2+hk+k^2\right)}{3a^2} + \frac{l^2}{c^2}\right] \tag{2.2}$$

$$V = \frac{\sqrt{3}}{2}a^2c \tag{2.3}$$

$$D = \frac{K\lambda}{\beta cos\theta} \tag{2.4}$$

$$\epsilon = \frac{\beta}{4tan\theta} \tag{2.5}$$

$$\chi D = \frac{ZW}{N_a V} \tag{2.6}$$

where θ (in degree) is the Bragg angle, λ is the x-ray wavelength (1.5406Å), (*hkl*) are the miller indices, *K* is the constant which is taken as 0.89 assuming the spherical shape of crystallites, β (in radian) is the full-width at half maxima calculated by $\left(\beta^2_{observed} - \beta^2_{instrument\ (Si)}\right)^{1/2}$, *Z* is the number of molecules per unit cell, *W* is molecular weight, N_a is Avogadro's number.

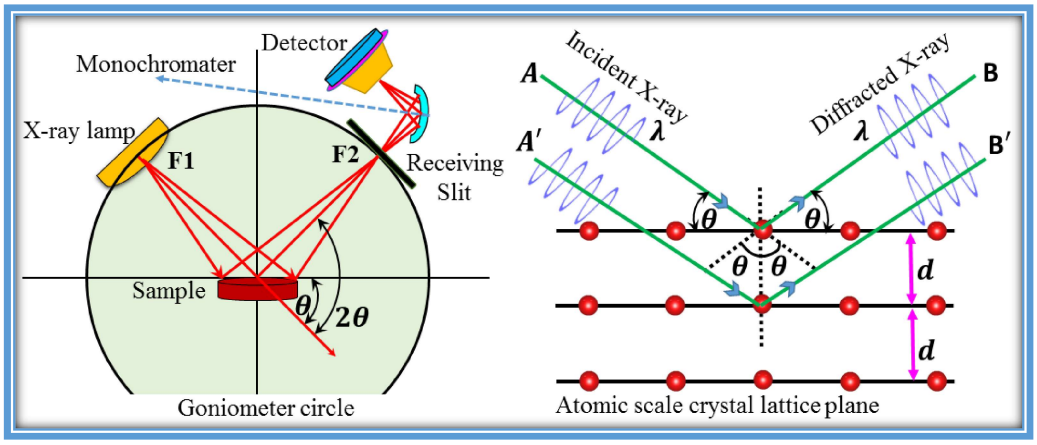

Figure 2.5 *Schematic representation of Bragg-Brentano geometry (Ray diagram of XRD) and Bragg's law.*

2.2.3 Fourier Transform Infrared Spectroscopy (FTIR)

Fourier transform infrared (FTIR) is the interaction analysis of infrared radiation with the particle as a function of photon frequency. FTIR characteristic analysis ensures the completion of a reaction between constituents and the phase formation after calcination. It also provides information about the vibration and rotation of chemical bonds present in the material. A schematic representation of FTIR spectroscopy is shown in Fig. 2.6. In this spectroscope, an IR source is used to emit infrared energy, which is allowed to pass through the aperture that controls the amount of infrared (IR) energy. Then, IR radiation passes

through the interferometer, which guides the radiation to incident on material precisely with the help of a beam splitter and mirror. When the material is exposed to IR radiation, atoms absorb the radiations at frequencies comparable to their vibrational modes. The scattered radiations from the material are collected by the detector, and the Fourier transform is applied to the spectrum, which is used for further interpretation. The corresponding spectrum as a function of IR radiation frequency is used to identify the characteristic features of material. The IR spectrum can be fragmented into two regions; functional group region and fingerprint region. The fingerprint region typically includes bending vibrations. While stretching vibrations are found in the functional group region, hence these vibrations are the main region of interest for bond determination. In FTIR spectra, a reverse relationship exists between the wavenumber and atomic weight of the molecule according to Eq. (2.7),

$$\nu = \frac{1}{2\pi l}\left[\frac{q}{\mu}\right]^{1/2} \tag{2.7}$$

$$\mu = \frac{W_{a_O}\times[(12-x-y)W_{a_{Fe}}+xW_{aNi}+yW_{a_{Al}}]}{W_{a_O}+[(12-x-y)W_{a_{Fe}}+xW_{aNi}+yW_{aAl}]} \tag{2.8}$$

where ν is the wavenumber, l is velocity of light, q is the force constant of the bond, μ is the effective mass of atoms, W_a is the atomic weight.

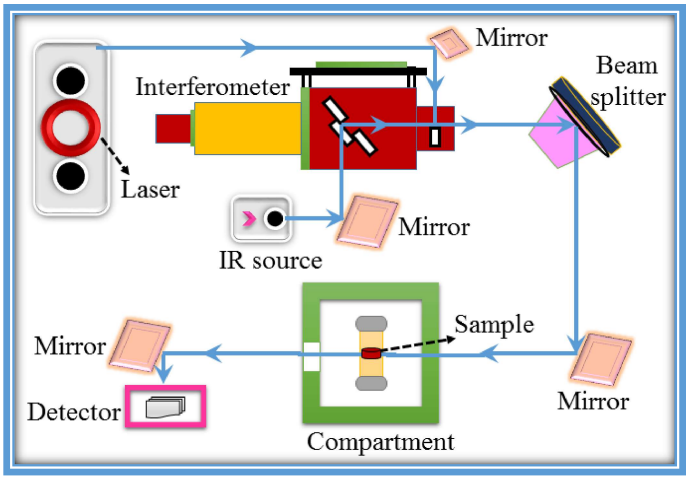

Figure 2.6 *Schematic representation of Fourier transform infrared spectroscopy.*

In the present work, FTIR spectrums of desiccated calcined powders were recorded in the 4000-400 cm^{-1} range by Perkin Elmer BXIII FTIR spectrometer in transmittance mode. The vacuum-dried IR-grade KBr (potassium bromide) was used to dilute the sample. In M-type hexaferrite, the absorption band between 400-500 cm^{-1} is caused by the Fe^{3+}-O^{2-} interaction at octahedral site, while absorption band between 500-700 cm^{-1} is resulted from the Fe^{3+}-O^{2-} interaction at tetrahedral site. The bond length of metal-oxygen (*r*), i.e., Fe-O was calculated by Eq. (2.9).

$$r = \left[\frac{17}{q}\right]^{1/3} \tag{2.9}$$

2.2.4 Scanning Electron Microscopy (SEM)

Scanning electron microscopy (SEM) uses the electron beam to form an image of material with information of surface morphology, foreign particle, residues etc. A schematic representation of scanning electron microscope is shown in Fig. 2.7. In this microscope, the tungsten filament is used to emit the electron beam thermionically. These electron beams are drawn towards the anode, then two successive condensers and objective lens are used to focus the beam with a fine spot size (~50 Å). Scanning coils are placed at the objective lens that reflects the electron beam either linearly or in a raster way over the material. The bombardment of electron beam caused to dislodge electrons from the sample where the electron interaction volume can be assumed like a teardrop shape, as shown in Figure 2.8. The secondary electrons (SE) are collected by the positively biased detector, which is then translated into the signal, amplified, and results in the topographic image of the sample. Backscattered electrons (BSE) possess more energy than SE, and BSE increases monotonically with the atomic no. Z of element (~ $0.05\sqrt{Z}$). It is helpful to differentiate one material from another.

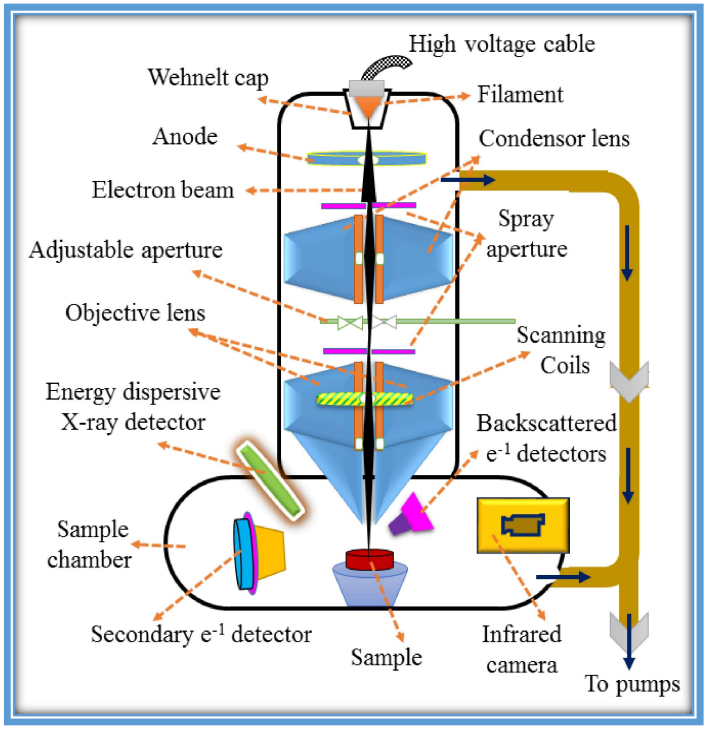

Figure 2.7 *Schematic representation of scanning electron microscope.*

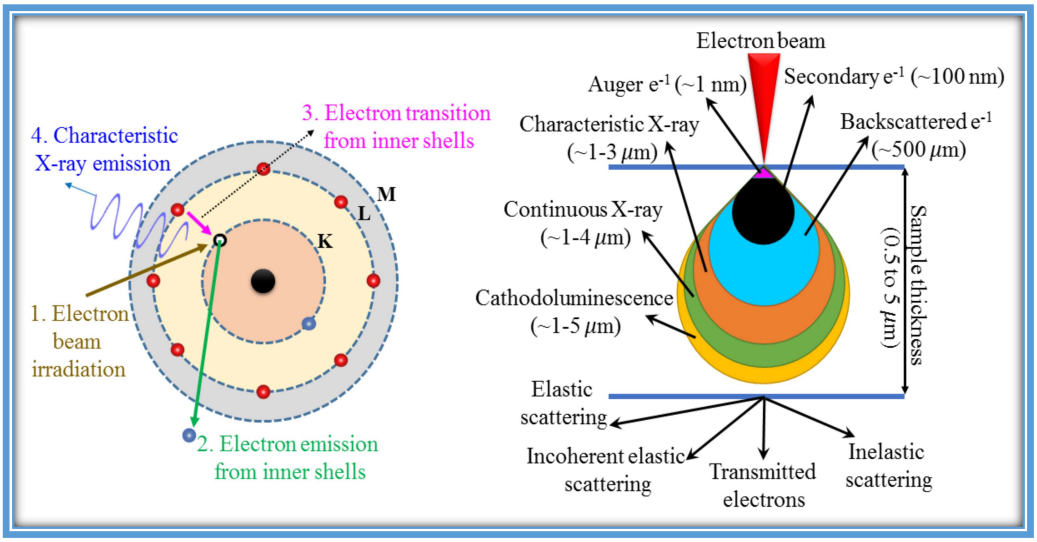

Figure 2.8 *Schematic representation of electron interaction with sample along with different generated signals.*

Energy dispersive x-ray spectroscopy (EDS) is an equipment equipped with the SEM, which gives information of compositional elements. Due to the unique atomic structure of each element, unique characteristic x-rays are emitted by the element. When high energy beam is focused on the sample, some inner core electrons may excite and

dislodge from the inner shell resulting in electron vacancy, as represented in Fig. 2.8. When this electron vacancy is filled by electron of the outer higher energy shell, energy difference of involved shells is released in the form of characteristic x-ray. The characteristic x-ray is used to identify the presence of different elements in the sample. The EDS spectrum displays peaks, where each peak is unique to an atom and relates to a single element.

In the present work, scanning electron microscopy SEM ZEISS, EVO 18–2045 equipped with energy-dispersive x-ray spectroscopy EDS was used for the elemental and morphological information of samples.

2.2.5 Bulk Density and Porosity

The Bulk density of all samples is estimated by the well-known Archimedes' methodology. It was used to evaluate the bulk density of samples according to Eq. (2.10) and porosity was estimated by Eq. (2.11).

$$\text{Bulk Density} = \frac{Dry\ weight}{Soaked\ weight - Suspended\ weight} * 100 \quad (2.10)$$

$$\text{P (\%)} = \frac{X-ray\ density - bulk\ density}{x-ray\ density} * 100 \quad (2.11)$$

2.2.6 Superconducting Quantum Interference Device (SQUID) Magnetometer

Superconducting Quantum Interference Device (SQUID) magnetometer is the most sensitive and effective equipment for analyzing the magnetic properties of a material. It is used for high magnetic field, low-temperature, and high-temperature magnetic study of samples. It measures the overall magnetic moment of material in an absolute unit directly when exposed to a magnetic field. A simplified representation of the SQUID magnetometer is shown in Fig. 2.9. An uninterrupted power supply is necessary to maintain a continuous power supply to all the connected equipment. The power supply circuit and electromagnets

are cooled with the water chiller to avoid overheating. A sample is fixed at the lower end of a non-magnetic quartz rod. After the calibration, the program of measuring sequences is run. The sample-mounted quartz rod is attached to a head drive that causes the vibration in the sample at the set amplitude and frequency. A closed-cycle Helium refrigerator and temperature sensor together contribute to cooldown the sample. The sample chamber is thermally attached to the cold head motor, which is connected to a Helium compressor. Dry helium gas is indorsed to flow continuously in the sample chamber for good thermal contact and temperature uniformity over sample. A cryostat is used in this system to recondense Helium (He) directly. A hall probe is placed between the pickup coil that measures the magnetic field with output capabilities. A temperature sensor is used to control the temperature variation during magnetic measurement. It is adequately shielded from the ambient environment and the magnetic field generated by the electromagnet.

The working principle of SQUID is schematically signified in Fig. 2.10. It is based on one/two parallel Josephson junctions in a loop. A supercurrent is built with a maximum critical value of I_c without any voltage across the Josephson junction. The supercurrent continuously flows through the weak link across the Josephson junction via tunneling of cooper pairs. Superconducting pickup coils are the main detection coil, which is configured as an II-order gradiometer. When the sample is allowed to vibrate under a magnetic field, a change in magnetic flux occurs. During the magnetic measurement, when a sinusoidal (up and down) movement is induced in the sample through a mechanical vibrator (head drive), it produces an alternating magnetic flux within the superconducting pickup coil, which is fixed at the pole piece of electromagnets. The pickup coil and SQUID antenna together transfer the magnetic flux from the sample to an rf SQUID device. The rf SQUID is a magnetic flux-to-voltage converter device, which is placed away from the sample in a liquid Helium bath. The amplitude of the generated signal is proportional to the vibrating

amplitude, vibration frequency, and magnetic moment of sample. Further, the voltage from the rf SQUID is amplified by electronic devices, and the signal portion resulting from the magnetic moment of sample is directly recorded for data analysis.

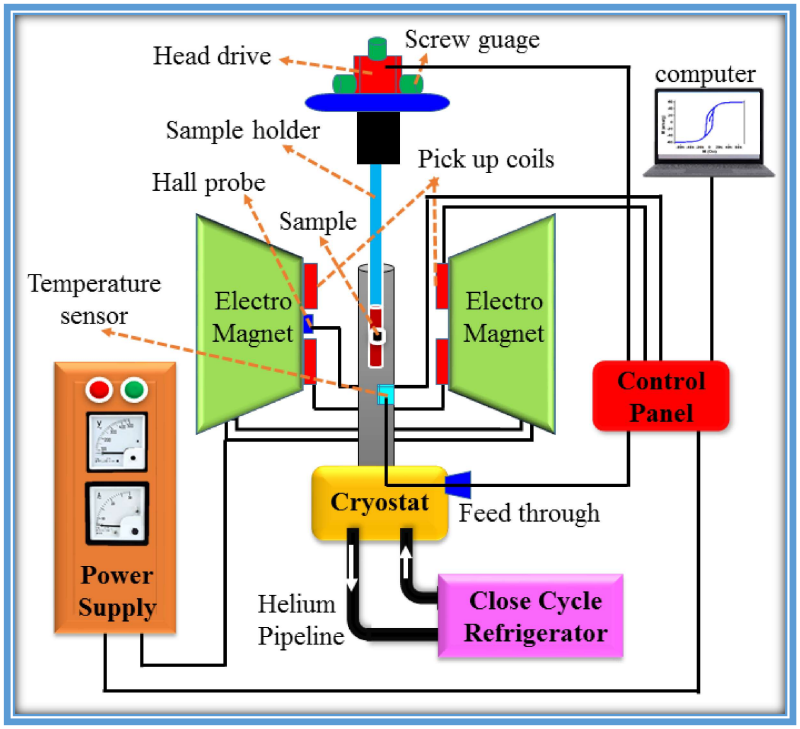

Figure 2.9 *A simplified representation of the SQUID magnetometer.*

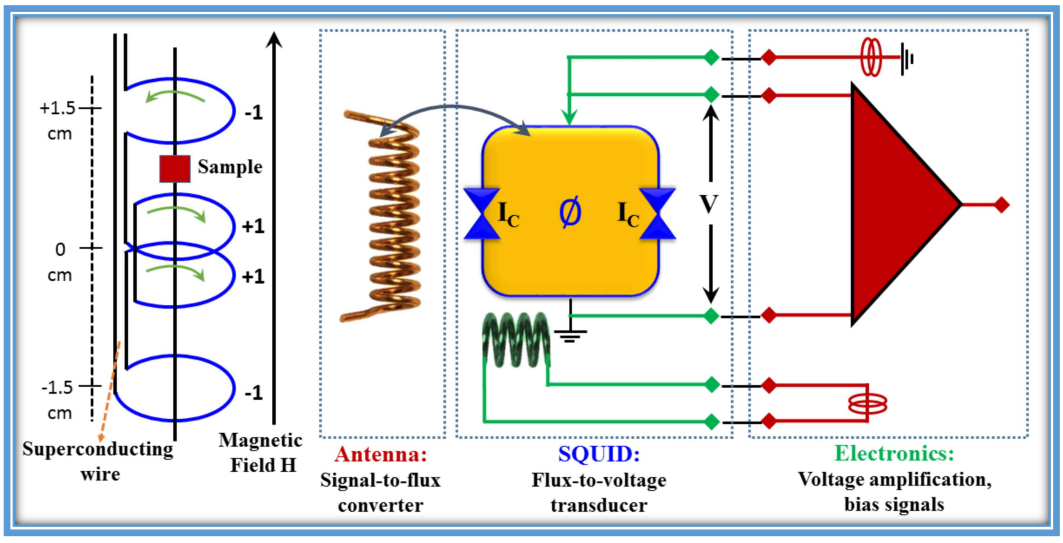

Figure 2.10 *Schematic representation of the working principle of SQUID.*

In the present work, the magnetic moment variation as a function of the applied magnetic field and applied temperature was recorded by the SQUID magnetometer (Quantum design, Model: MPMS 3, EM-QM, USA), which is capable of producing a maximum applied magnetic field of 70 kOe (7 Tesla). Its sensitivity is $< 1\times10^{-8}$ emu ($\leq$ 2500 Oe) and $< 8\times10^{-8}$ emu (> 2500 Oe). It permits the magnetization measurement in 1.8-400 K, and the oven option allows magnetization measurement in 315-1000 K. For high-temperature measurement (>300 K), an oven assembly replaces cryostat, and an alumina sample holder was used. Here are some formulae that were used in the magnetic analysis,

$$\mu_B = \frac{Molecular\ weight \times M_s}{5585} \tag{2.12}$$

$$H_c = \alpha\left(\frac{2K}{M_s}\right) \tag{2.13}$$

$$K_{eff} = M_s\sqrt{\left(\frac{15\gamma}{4}\right)} = \frac{M_s H_a}{2} \tag{2.14}$$

$$H_c = \alpha H_a - \frac{N}{\mu_o}(B_r + J_s^0) \tag{2.15}$$

where μ_B is the Bohr magnetron number, M_s is the saturation magnetization, H_c is the coercivity, α is the grain size factor, K_{eff} is the effective magnetocrystalline anisotropy, γ is obtained from the slope of M vs. $1/H^2$ plot, H_a is the magnetocrystalline anisotropy field, N is the grain demagnetization factor, μ_o is the free space permeability, and J_s^0 is the saturation polarization.

2.2.7 Impedance Analyzer

The impedance analysis is used to confirm different phenomena like electric conduction, ferroelectricity, dipolar ordering, and relaxation. The schematic representation of room-temperature impedance analyzer is shown in Fig. 2.11. The setup consists of an LCR meter connected to the sample holder through four BNC connectors. The measurement is done by the arrangement of parallel plate capacitors working in the four-

terminal method. The top metallic plate is spring loaded, which ensures the possible adjustment for good electrical contact with the sample. The connection is such that the top plate is coupled to I_H, V_H while bottom plate is coupled to I_L, V_L.

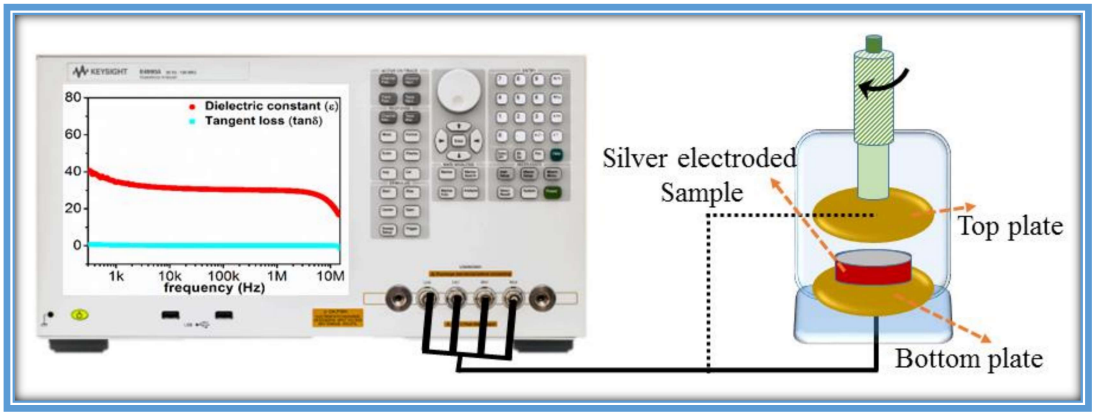

Figure 2.11 *Schematic representation of room-temperature impedance analyzer.*

In the present work, the impedance analyzer Keysight Technology (Model E4990A, 20 Hz to 20 MHz frequency range) was used for the room-temperature electrical study. Samples were prepared as cylindrical shape sintered pellets, which were painted with high-grade Silver paste at the top and bottom surfaces, followed by drying in an oven for 2 hrs at 120°C. Then samples were cooldown to room temperature and tested by the impedance analyzer. The capacitance value and tangent loss ($tan\delta$) as a function of frequency were directly given by the instrument software. A further dielectric study was performed with the recorded data by applying the following formulae,

$$\varepsilon_r = \frac{Cd}{\varepsilon_o A} \tag{2.16}$$

$$\rho = \frac{1}{\omega * \varepsilon_0 * \varepsilon_r * tan\,\delta} \tag{2.17}$$

$$\sigma = {}^{1}/_{\rho} \tag{2.18}$$

where ε_r is relative dielectric permittivity, ε_o is free space dielectric permittivity, C is the capacitance, d is the height between the silver electrodes, A is the cross-sectional area, ρ is ac-resistivity, and σ is ac-conductivity.